

Influence of heat treatment on microstructure and passivity of Cu–30Zn–1Sn alloy in buffer solution containing chloride ions

U TABRIZI¹, R PARVIZI¹, A DAVOODI^{2,*} and M H MOAYED¹

¹Materials and Metallurgical Engineering Department, Faculty of Engineering, Ferdowsi University of Mashhad, Mashhad 91775-11, Iran

²Materials Engineering Department, Faculty of Engineering, Sabzevar Tarbiat Moallem University, Sabzevar 397, Iran

MS received 20 August 2009; revised 29 June 2011

Abstract. Tin as an alloying element is of great interest in brasses for dezincification impediment. In this paper, Cu–30Zn–1Sn alloy was submitted to three different heat treatments, viz. A (heating up to 800 °C for 20 h, held at 200 °C for 20 h in salt bath and air cooled), B (heating up to 800 °C for 20 h and water quenched) and C (heating up to 600 °C for 20 h and water quenched). The influence of heat treatment on microstructure was evaluated by OM and SEM–EDS analysis. The corrosion resistance in buffer solution (pH 9), H₃BO₃/Na₂B₄O₇·10H₂O, with various concentrations of chloride ions was evaluated by potentiodynamic polarization curves and compared with multi-component Pourbaix diagrams. A correlation between the heat treatment, microstructure and passivity of the heat treated samples was observed. The results indicated that all heat treatment procedures led to formation of α , and γ -Sn-rich phases as microstructure constituents with a small fraction of β' phase in A. Sn-rich phase appears in grain boundaries and its morphology was slightly changed due to heat treatment. Beneficial influence of low concentration chloride ions on passivity was associated with the formation of copper oxides/hydroxide and chloride complexes. Deterioration was observed at concentrations higher than 0.05 M NaCl due to accelerated dissolution of copper by formation of CuCl₂⁻. As a result of dezincification process, preferential corrosion attack and copper redeposition on α phase (matrix) were observed. However, Sn-rich (γ_1) phase in grain boundaries was not attacked due to SnO₂ formation. In buffer solution, the higher passivity current density in A was related to the presence of small amount of β' phase. On the other hand, in 1 M NaCl, lower critical current density for passivation in B and A (about two times lower than C) was attributed to the grain size effect.

Keywords. Brass; dezincification; corrosion; heat treatment effect; chloride attack.

1. Introduction

Copper and its alloys have wide industrial applications including marine environments. Brasses, as the most familiar category of copper alloys, are usually solid solution of α , $\alpha + \beta$ and β in Cu–Zn system with a maximum of 50% zinc (Jones 1992; Kabasakaloglu *et al* 2002; Sherif and Park 2006; Sherif *et al* 2007a, b). For a long time, it has been observed that brasses exposed to aerated water containing high concentrations of chloride ions undergo corrosion deterioration (Morales *et al* 1995a, b; Kabasakaloglu *et al* 2002; Sohn and Kang 2002; Asan *et al* 2005; Mamas *et al* 2005). Low corrosion resistance of brasses in this environment is due to a phenomenon called dezincification. Dezincification is mainly selective dissolution of zinc and dissolution and redeposition of copper (self-catalytic effect) and formation of porous copper oxide layer with loose structure

(Jones 1992). It has been suggested that at low potential, dezincification mechanism is preferential dissolution of zinc. While at intermediate potential, the alloy is dissolved by zinc and copper dissolution followed by copper redeposition, at high potential both zinc and copper are dissolved without copper redeposition (Heidersbach and Verink 1972). If the alloy potential in the electrolyte is close to the copper oxide formation potential, copper oxides as corrosion products are produced and in the presence of sufficient chloride ions, alloy dissolution occurs by formation of copper chloride complexes (Zou *et al* 1997; Scendo 2007). To avoid or decrease dezincification, three methods are used (i) replacing $\alpha + \beta$ brass by α brass (since β -phase enriched by Zn has lower electrochemical potential as compared to α phase enriched by copper), (ii) performing heat treatment on two-phase $\alpha + \beta$ brass and transforming it to a single α brass and (iii) adding a small fraction of suitable alloying elements including arsenic, antimony, boron, phosphorus, tin and aluminum (Polunin *et al* 1982; Toivanen *et al* 1985; Newman *et al* 1988; Crousier and Bimaghra 1989; ASM 2004c). Among these methods, the third one is the most efficient. Dezincification of α brass is decreased in Naval (71Cu–28Zn–1Sn–0.1As) alloy brass

* Author for correspondence (adavoodi@kth.se)

by adding tin element and it has been suggested that tin forms acicular oxide particles which behaves as passive layer and reduces anodic current and corrosion penetration. This passive layer inhibits copper redeposition and/or preferential zinc dissolution (Sohn and Kang 2002). This inhibition continues up to the potential of CuCl formation. Formation of passive film on two-phase brass containing tin initiates on α phase surface and propagates on β phase surface and inhibits both zinc preferential dissolution and copper redeposition (Sohn and Kang 2002). Tin as an anti-corrosion alloying element is of great interest in brasses for dezincification obstruction. However, in spite of vast researches studying the effect of tin on the improvement of dezincification resistance, the influence of heat treatment on corrosion (particularly passivity) behaviour of brass containing tin element was less investigated. In this work, effect of various heat treatments on microstructure, corrosion resistance and passivity of Cu–30Zn–1Sn alloys in a boric acid–disodium tetraborate ($\text{H}_3\text{BO}_3/\text{Na}_2\text{B}_4\text{O}_7 \cdot 10\text{H}_2\text{O}$) buffer solution with various concentrations of chloride ions (NaCl) at a pH of 9 is investigated using potentiodynamic polarization, metallographical examination and SEM-EDX analysis of selected phase. Different heat treatments were used to obtain desired microstructure and morphology.

2. Materials and experimental

Raw materials were produced by direct melting of Cu–30Zn brass alloy in a crucible and pure Sn at 1050 °C to obtain an alloy with the composition, Cu–Zn30–1Sn. Cast alloy then homogenized at 800 °C for 20 h in heat treatment furnace and quenched in water (ASM 2004a). Then, the specimens were cut and 50% hot deformation was performed at 700 °C followed by air cooling. Finally, three different heat treatment procedures in natural atmosphere were applied as described below (ASM 2004b).

Procedure A. The specimen was heated up to 800 °C for 20 h and then held at 250 °C for 20 h in salt bath (the molten salt composition was $\text{NaNO}_2(40\%) + \text{NaNO}_3(10\%) + \text{KNO}_3(50\%)$) and finally furnace cooled.

Procedure B. The specimen was heated up to 800 °C for 20 h and then quenched in water.

Procedure C. The specimen was heated up to 600 °C for 20 h and then quenched in water.

For corrosion studies, pure sodium chloride (NaCl), boric acid (H_3BO_3) and disodium tetraborate ($\text{Na}_2\text{B}_4\text{O}_7 \cdot 10\text{H}_2\text{O}$) with Merck quality were used to obtain a buffer solution at pH 9 (Morales *et al* 1995a, b, 1998) with various chloride concentrations. For metallographical examination, $\text{FeCl}_3(7.5\text{gr}) + \text{HCl}(30\text{ml}) + \text{H}_2\text{O}(120\text{ml})$ was used as an electrochemical etchant. Electrochemical etching was performed

in Electropol-5 Struers instrument with 0.1 A/cm², 8 V, for 15 s (ASM 2004a, b, c). To study the surface morphology, SEM (model LEO 1450VP with EDS-Oxford 7353) was used. The samples were ground up to 1200 SiC abrasive pad, polished by 1 μm diamond paste, degreased by acetone in an ultrasonic cleaner, washed using distilled water and dried by hot air. All corrosion experiments were done at ambient temperature. For potentiodynamic measurements, a potential range from 50 mV below corrosion potential up to the 1500 mV above it with a scan rate of 1 mV/s was used. Prior to potentiodynamic polarization measurements, the samples were held at their free potential for 15 min to stabilize the potential. To observe the corrosion attack morphology, all samples were polarized potentiostatically, +230 mV, above the corrosion potential for 900 s. A triple electrode configuration was used for electrochemical measurements including platinum wire as a counter, saturated calomel as a reference and sample as the working electrodes, respectively. All potentials were plotted against saturated calomel reference electrode (SCE).

In addition, to elucidate the chloride ions effects on corrosion behaviour of investigated alloy, thermodynamics calculations were performed and multi-component Pourbaix diagram including chloride and borate species were obtained (Medusa 2009). Thermodynamics results based on Pourbaix diagram were compared with kinetic results based on Evans diagrams, i.e. potentiodynamic polarization curves.

3. Results and discussion

3.1 Microstructure

Considering ternary alloy phase diagrams of Cu–Zn–Sn (Hansen and Anderko 1958; Effenberg and Ilyenko 2006), equilibrium solidification of Cu–30Zn–1Sn sample follows $L \rightarrow L + \alpha \rightarrow L + \alpha + \beta + \gamma \rightarrow \alpha + \beta + \gamma$ (γ is a Sn-rich phase) sequence. However, non-equilibrium heat treatment procedures of A, B and C led to formation of α , β' (an ordered β phase) and Sn-rich phases as microstructure constituents. By using the etchant mentioned in previous section, β' phase appears darker than α phase (ASM 2004a). Figure 1 shows microstructure of Cu–30Zn–1Sn after heat treatment procedure A. The matrix appears in α and a small amount of γ (light blue colour) phase appears in grain boundaries in conjunction with tiny interconnected β' phase. The grains are rounded due to the second stage of heat treatment procedure A. SEM image shows details of needle-like feature of secondary phases. EDS analysis also confirms the presence of Sn-rich phase in grain boundaries. Figure 2 represents the microstructure of Cu–30Zn–1Sn after heat treatment procedure B. The microstructure includes a matrix of α , with filaments of α phase coincident with γ phase appearing in grain boundaries. The grain boundaries are sharper and heat treatment B led to noticeable change in morphology and

amount of α and γ phases as compared to A (figure 1). Moreover, here, the β' phase does not exist. Figure 3 shows microstructure of Cu–30Zn–1Sn after heat treatment procedure C. The microstructure includes matrix of the single α phase and γ as the secondary phase. Noticeably, due to lower heat treatment temperature, the grain size slightly decreases in C as compared to A and B. While in A, β' phase is surrounded by γ phase, in B and C, γ phase is enfolded by α phase.

3.2 Multi-component Pourbaix diagram

To illustrate the influence of chloride ions on phase stability regions, thermodynamics calculations were performed and multi-component Pourbaix diagram including chloride and borate species were drawn as shown in figures 4 and 5 (Medusa 2009). Figure 4 presents the multi-component Pourbaix diagrams for copper in pure water and aqueous

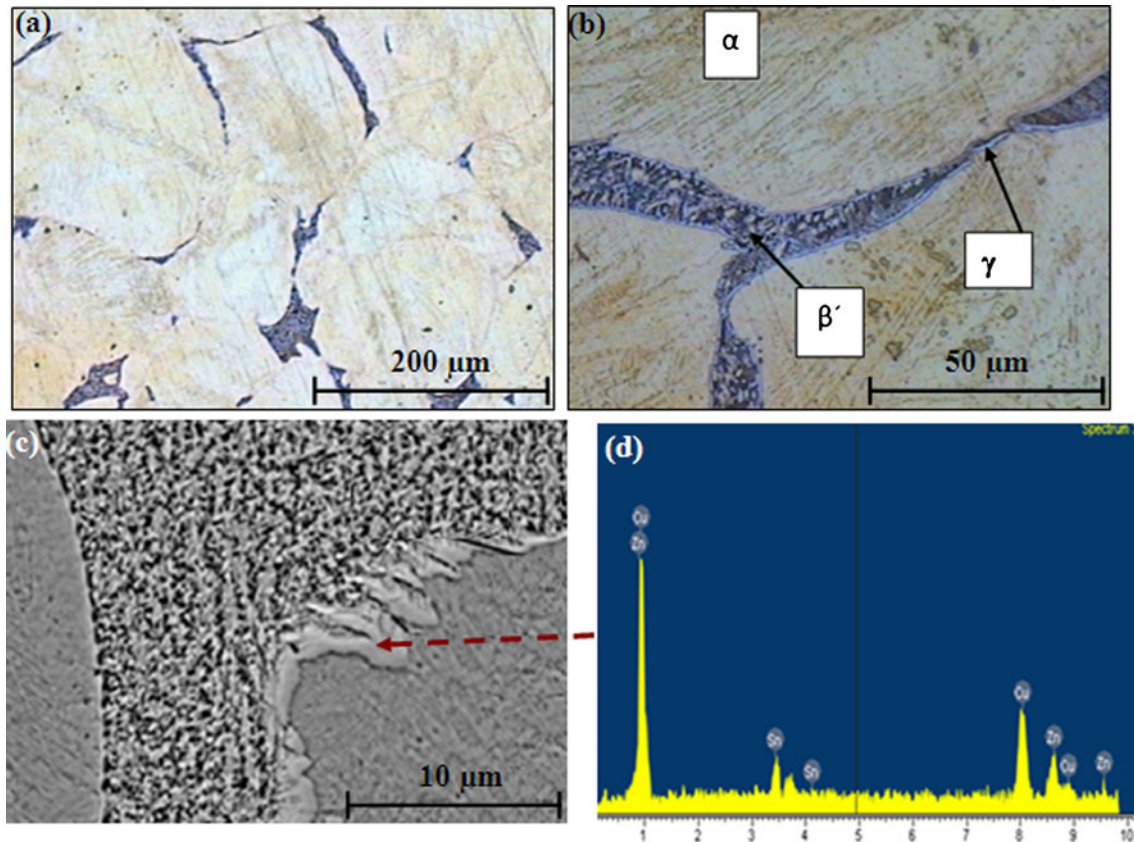


Figure 1. (a) and (b) Microstructures of Cu–30Zn–1Sn after heat treatment procedure A and (c) SEM image and (d) EDX analysis of indicated Sn-rich phase.

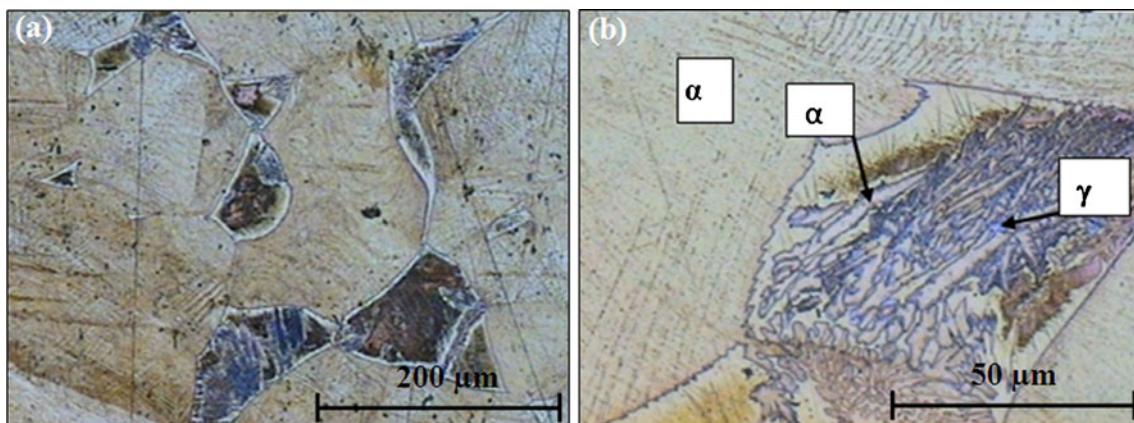


Figure 2. (a) and (b) Microstructure of Cu–30Zn–1Sn after heat treatment procedure B.

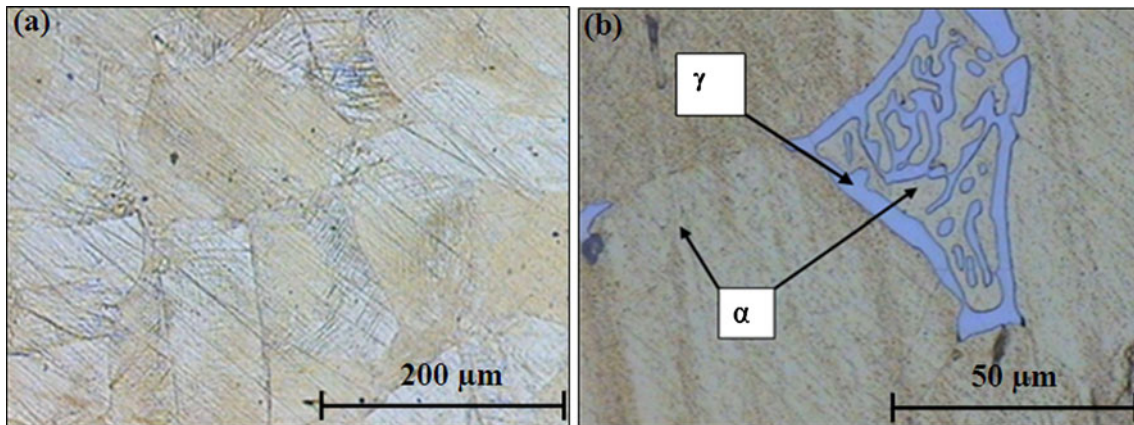


Figure 3. (a) and (b) Microstructure of Cu-30Zn-1Sn after heat treatment procedure C.

solutions with 0.05 and 1 M chloride concentrations. Without chloride ion, increasing the potential at pH 9 led to the formation of Cu_2O and consequently CuO compounds (figure 4(a)). It should be noticed that in aqueous solution, copper oxides may be presented in the form of copper hydroxide, $\text{Cu}(\text{OH})_2$ (Jones 1992; Milosev *et al* 2006). At 0.05 M NaCl, formation of CuCl_2^- in acidic and neutral environments is predicted, but its presence at pH 9 could not be reported (see figure 4(b)). Interestingly, at pH 9, in 1 M NaCl, Pourbaix diagram predicts a higher copper affinity to the chloride ions, leading to CuCl_2^- formation instead of Cu_2O . Figure 5 represents multi-component Pourbaix diagrams for zinc and tin in aqueous solutions with and without NaCl. In 0–0.05 M NaCl solution, at pH 9, formation of both ZnOH^+ and $\text{Zn}(\text{OH})_2$ is predicted. Since stability regions of these two components are starting from significantly lower than the copper oxide formation (starting from -1 V vs SHE), passivity on alloy surface can be most likely associated to the $\text{Zn}(\text{OH})_2$ formation at lower potentials and to the Cu_2O and CuO formation in conjunction with previously formed zinc hydroxide at higher potentials. At high Cl^- concentration, formation of both zinc hydroxychloride compound, ZnClOH , and zinc hydroxide, $\text{Zn}(\text{OH})_2$, is possible (see figure 5(b)). Therefore, passivity at high Cl^- concentration can be mainly associated to ZnClOH and $\text{Zn}(\text{OH})_2$ surface constituents (see figure 5(b)). While thermodynamic assessment reveals that Cu_2O cannot be formed at high Cl^- concentration, only CuO can incorporate in passive layer at high potential regions. With regard to tin alloying element, it can be seen that at present in aqueous solution, tin produced a stable surface tin oxide (SnO_2 layer) leading to passivation occurrence in large potential and pH domain as shown in figure 5(c). However, according to the metallographical observation in previous section, tin is localized at grain boundaries as γ phase and therefore, during corrosion, SnO_2 surface layer could protect the attack only on the grain boundary regions where it is present.

It must be mentioned that in spite of usefulness of Pourbaix diagrams, they are subject to several important limitations such as equilibrium assumption, application to

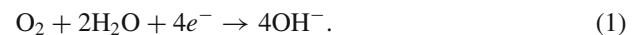
single elemental metals only and not to alloys and giving no information on actual corrosion rates. Moreover, they do not provide any information on actual surface oxide protective properties and do not consider localized corrosion by chloride ion (Jones 1992).

Since kinetics parameters influence on passive layer integrity (such as barrier characteristics) cannot be estimated by Pourbaix diagrams (Jones 1992), Evans diagrams based on potentiodynamic polarization measurements are presented in the next section.

3.3 Potentiodynamic polarization results

Figure 6 shows potentiodynamic polarization measurements of Cu-30Zn-1Sn alloy after heat treatment A in boric acid–disodium tetraborate buffer solution at pH 9 containing various chloride concentrations. In $\text{H}_3\text{BO}_3/\text{Na}_2\text{B}_4\text{O}_7 \cdot 10\text{H}_2\text{O}$ buffer solution and buffer solution plus low chloride concentrations (up to 0.05 M NaCl), the alloy reveals passivity characteristics with wide passivity domain more than 1000 mV. Moreover, decrease in passivity current density to <1 $\mu\text{A}/\text{cm}^2$ (more than 3 times as compared to buffer solution) indicates that the passivity integrity is improved by adding chloride ions at 0.001 and 0.01 M concentrations.

It is well known that the cathodic reaction occurred on copper alloys surface in aerated NaCl solutions because of oxygen reduction (Sherif and Park 2006; Sherif *et al* 2007a, b, 2008):



Since, in this solution, zinc is either dissolved by formation of soluble hydroxide compound, ZnOH^+ , or produced $\text{Zn}(\text{OH})_2$ surface layer (figure 5 (a)); passivity can be mainly associated to both copper oxides, Cu_2O and CuO (at higher potentials), and zinc hydroxide, $\text{Zn}(\text{OH})_2$, formation on alloy surface (Milosev *et al* 2006; Sherif *et al* 2007a, b) probably by the following reactions



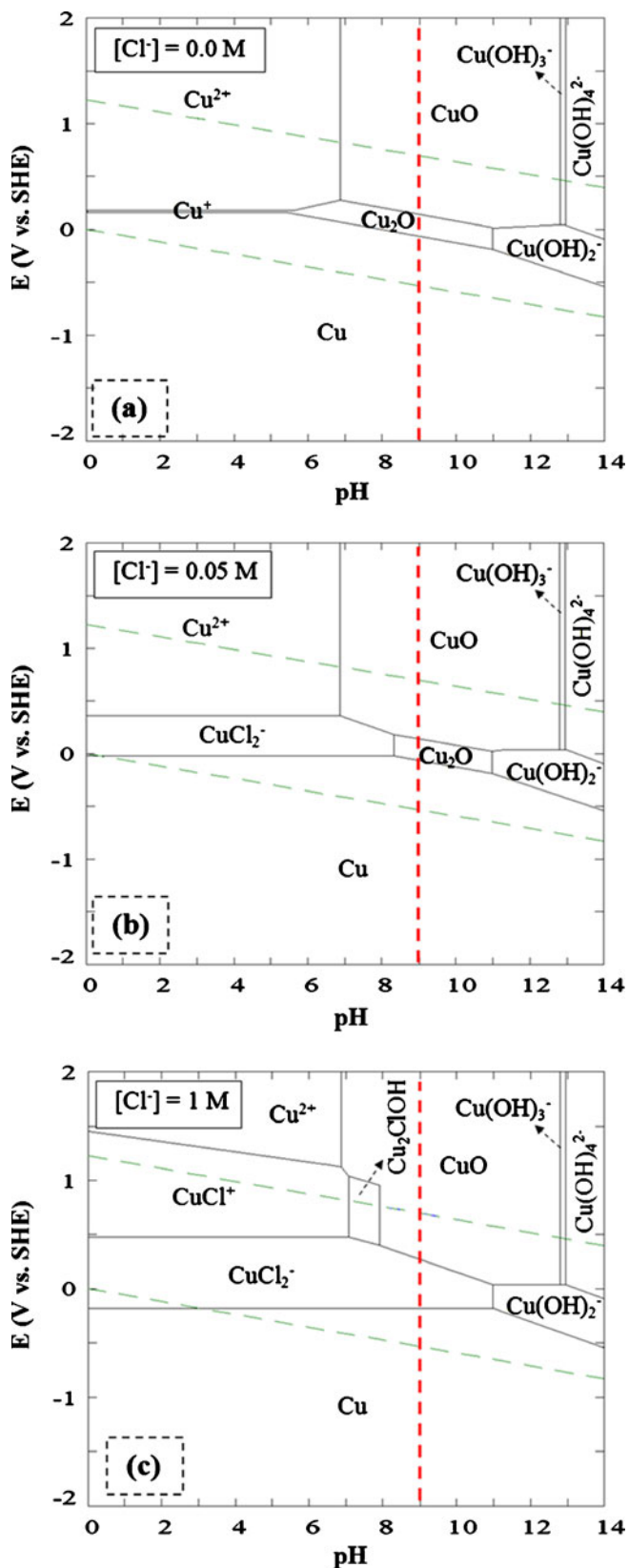


Figure 4. (a), (b) and (c) Pourbaix diagrams of copper in 0.0, 0.05 and 1 M NaCl aqueous solution.

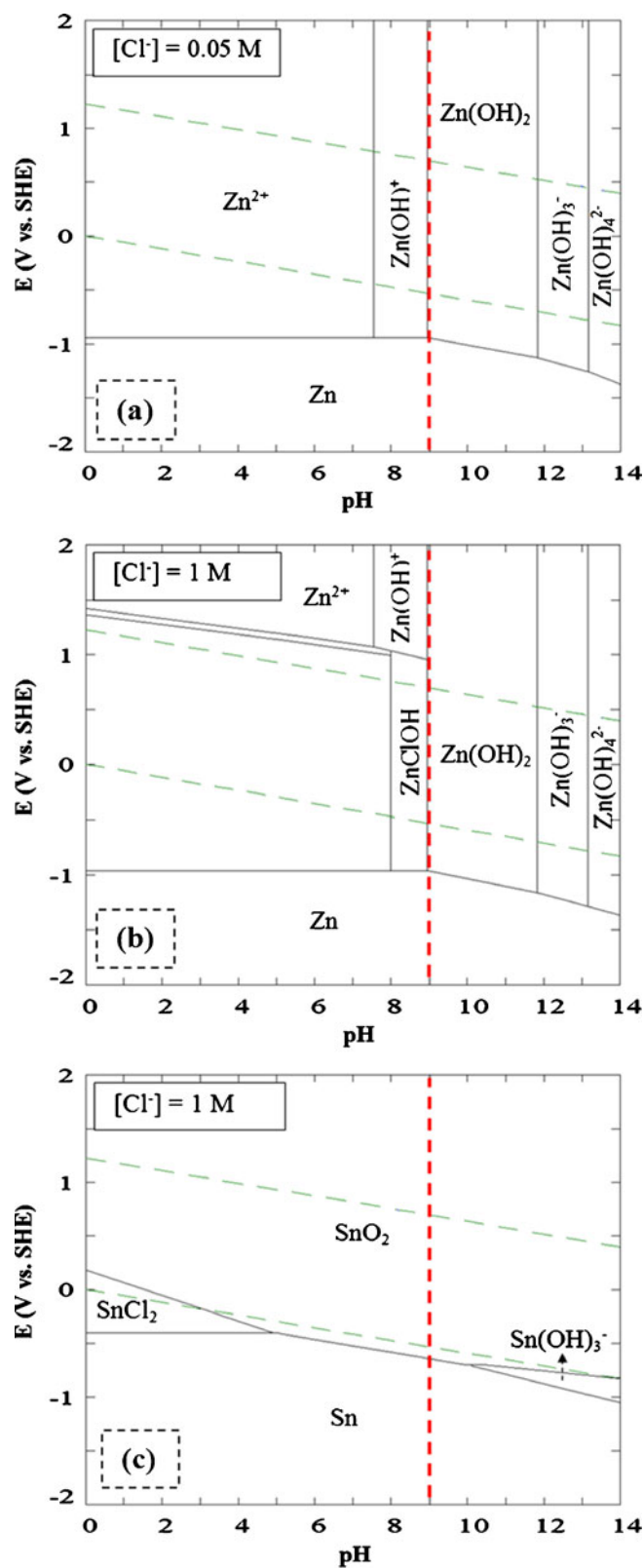


Figure 5. (a) and (b) Pourbaix diagrams of zinc in 0.05 and 1 M NaCl and (c) Pourbaix diagram of tin in 1 M NaCl aqueous solution.

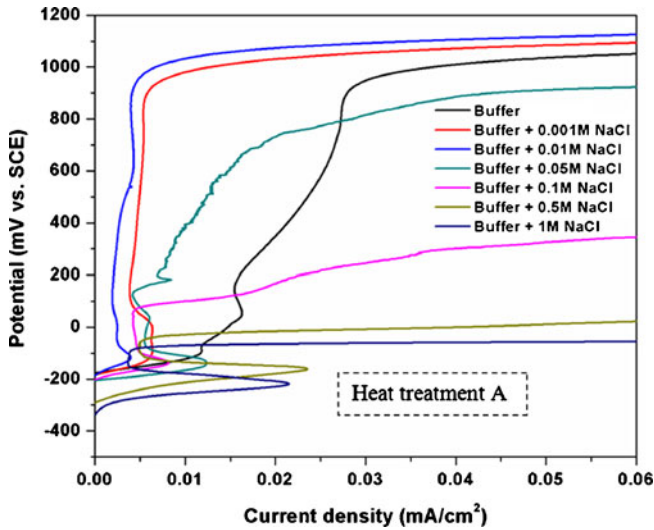
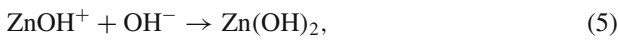
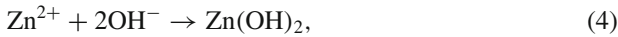


Figure 6. Potentiodynamic polarization curves of Cu-30Zn-1Sn alloys after heat treatment A in $\text{H}_3\text{BO}_3/\text{Na}_2\text{B}_4\text{O}_7 \cdot 10\text{H}_2\text{O}$ buffer solution, pH 9, containing various chloride concentrations.



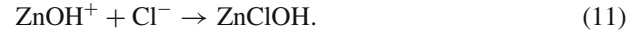
Beneficial influence of chloride ions on passivity, at low concentrations, can be attributed to probable CuCl surface layer formation which has been reported previously (Milosev *et al* 2006; Sherif and Park 2006; Sherif *et al* 2007a, b, 2008). In other words, presence of small amounts of Na^+ and Cl^- ions at low concentrations facilitates the conditions for formation of surface copper oxide and zinc hydroxide compounds and copper chloride complex as passive layer on the sample surface. This indicates that chloride ions contribute most likely to the passive layer constituent and improve the passivity integrity.

By further increase in chloride ions concentration, the passivity domain diminished and pitting occurred, hence, the breakdown potential suddenly reached to the pitting potential at 100 mV in 1 M NaCl. In addition, passivity current density is also increased. This indicates that higher chloride ion concentrations destroyed the passive layer and deteriorated the passivity integrity by formation of soluble copper chloride complex according to the following possible reactions (Zou *et al* 1997; Mamas *et al* 2005; Milosev *et al* 2006; Sherif and Park 2006; Scendo 2007; Sherif *et al* 2007a, b, 2008)



Therefore, a critical chloride concentration between 0.01 and 0.1 M can be defined whereas at concentrations lower than that, the alloy undergoes a stable passivity.

Short domain passivity at high Cl^- concentration can be mainly associated to ZnClOH and $\text{Zn}(\text{OH})_2$ surface constituents (see figure 5(b)).



Although ZnClOH and $\text{Zn}(\text{OH})_2$ are relatively stable up to higher potentials, but they cannot protect the surface and deterioration of passivity is mainly due to copper dissolution (Jones 1992; Alfantazi *et al* 2009). In a previous study (Alfantazi *et al* 2009), formation of zinc hydroxychloride compounds was not considered in thermodynamic calculations which may be due to insufficient thermodynamics data base. No contribution of tin oxide can be observed since they are only present at grain boundaries. Tin may also contribute to the passive layer constituents. However, due to the applied heat treatment, no detectable tin was observed in the alloy based on EDS analysis performed on alloy matrix.

Figure 7 shows potentiodynamic polarization measurements of Cu-30Zn-1Sn alloy after heat treatment B in buffer solution, pH 9, containing various chloride concentrations. A similar trend as A was observed in which below a critical chloride concentration the passivity occurred. Passivity integrity can be essentially attributed to the formation of surface copper oxide layers (Morales *et al* 1995a, b, 1998). Figure 8 shows potentiodynamic polarization measurements of Cu-30Zn-1Sn alloy after heat treatment C. More or less similar results can be observed.

In summary, in all heat treatment conditions, increasing chloride concentration to a critical value destroys the passivity by increasing the current density and reducing the passivity domain. At high enough chloride concentrations, due to passivity breakdown pitting occurs. To elucidate the influence of heat treatment on passivity, figure 9 shows potentiodynamic polarization results of Cu-30Zn-1Sn alloy after heat treatment A, B and C in buffer solution containing 0

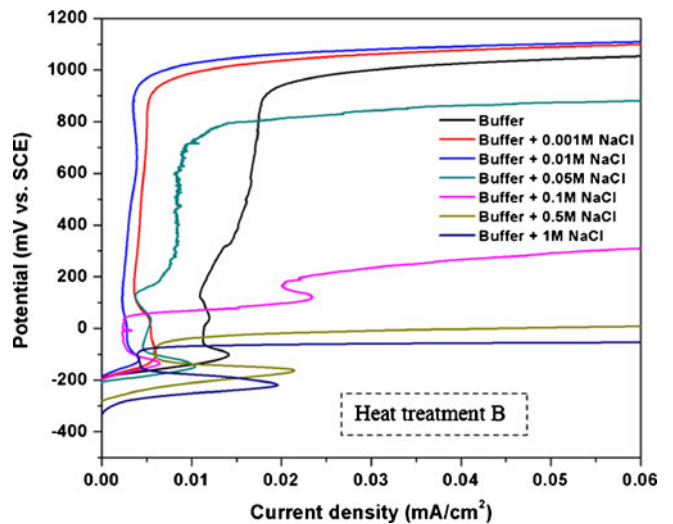


Figure 7. Potentiodynamic polarization curves of Cu-30Zn-1Sn alloys after heat treatment B in $\text{H}_3\text{BO}_3/\text{Na}_2\text{B}_4\text{O}_7 \cdot 10\text{H}_2\text{O}$ buffer solution, pH 9, containing various chloride concentrations.

and 1 M chloride concentrations. In figure 9(b), the critical current density for passivation, the passivity current density itself and the breakdown potential are the three parameters which can be used for comparison. In buffer solution, whereas the passivity is mainly associated to the Cu_2O and CuO formation, the higher passivity current density observed in A is likely related to the small amount of β' (with lower corrosion resistance as compared to α phase) which does not exist in B and C. Two anodic current peaks observed at -100 and $+50$ mV corresponded to Cu_2O and CuO formation, respectively (reactions (2) and (3)). Owing to a slightly smaller grain size in C results in higher critical current for Cu_2O formation. However, formation of CuO on A (particularly on β' phase surface), consumes slightly more current as compared to B and C conditions; the second peak at $+50$ mV.

In 1 M NaCl, the passivity current and breakdown potential (pitting potential) are similarly $4 \mu\text{A}/\text{cm}^2$ and -50 mV, respectively (see figure 9(b)). As described previously, short passivity domain due to pitting in 1 M NaCl is associated to the formation of copper chloride complex (reaction 5), followed by copper dissolution (reaction 6). Moreover, the critical current density for passivation in B and A series are appreciably less than C (about two times less). In other words, critical current density slightly decreases from $40 \mu\text{A}/\text{cm}^2$ in C to $20 \mu\text{A}/\text{cm}^2$ in A and B. Again, higher critical current density in C as compared to A and B can be attributed to microstructural differences such as grain size.

3.4 Corrosion attack morphology

Figure 10 shows the corrosion attacks on Cu–30Zn–1Sn alloys in heat treatment condition A. The preferential attack (pits) locations are mostly on α phase as matrix. No local corrosion attack is observed on Sn rich and β' phases. Re-deposited copper particles can also be observed (with $25 \mu\text{m}$

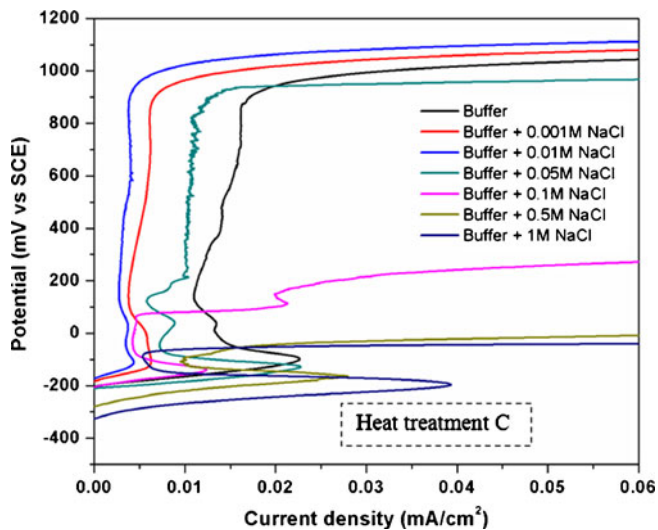


Figure 8. Potentiodynamic polarization curves of Cu–30Zn–1Sn alloys after heat treatment C in $\text{H}_3\text{BO}_3/\text{Na}_2\text{B}_4\text{O}_7 \cdot 10\text{H}_2\text{O}$ buffer solution, pH 9, containing various chloride concentrations.

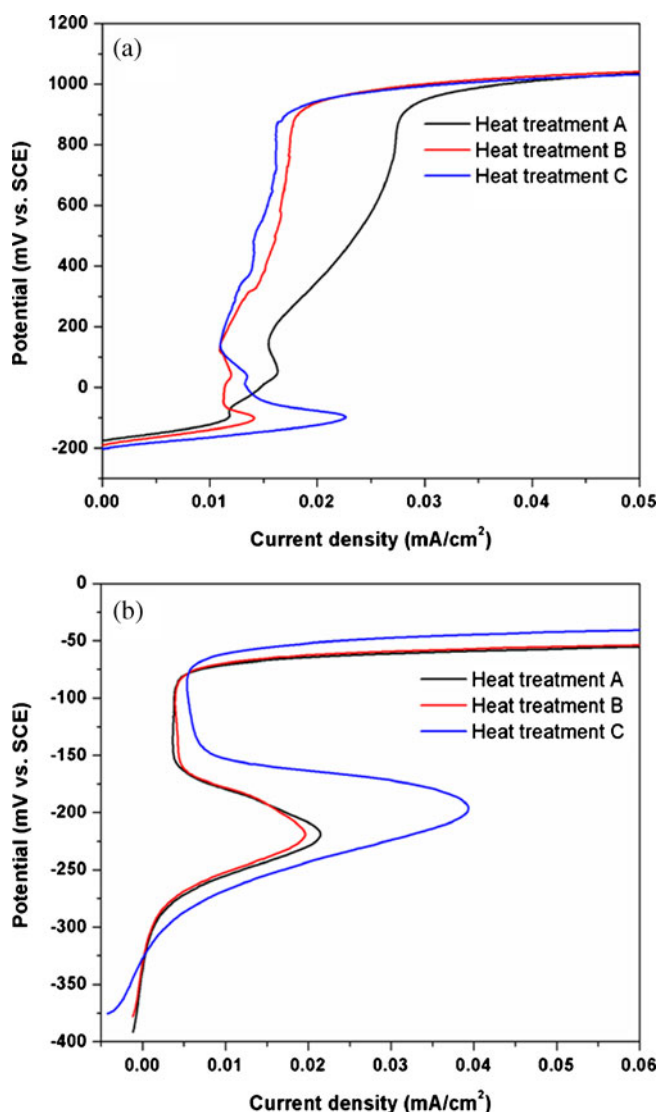


Figure 9. Potentiodynamic polarization curves of Cu–30Zn–1Sn alloys after heat treatments A, B and C in $\text{H}_3\text{BO}_3/\text{Na}_2\text{B}_4\text{O}_7 \cdot 10\text{H}_2\text{O}$ buffer solution, pH 9, containing (a) 0 and (b) 1 M NaCl.

in diameter) on α phase in matrix. This indicates that the corrosion mechanism at these conditions is preferential zinc dissolution, consequently copper dissolution and afterward redeposition of copper on the surface as the self-catalytic effect (Jones 1992). Figure 11 represents the corrosion attack on Cu–30Zn–1Sn in heat treatment condition C. Again, the preferential attack locations are on α -phase. Corrosion attacks were also observed on α -phase surrounded by γ -phase. The morphology (diameter) and numbers of pits are more or less similar at various heat treatments. Similar corrosion attack morphologies was observed in B (the results are not shown here). Since the Sn element was accumulated at grain boundaries as Sn-rich phase, it seems that adding Sn, as an alloying element, does not significantly improve the passivity of α -phase in matrix (the results on the sample without Sn (Cu–30Zn alloy) were not shown here) which is in contrast with previously suggested mechanism

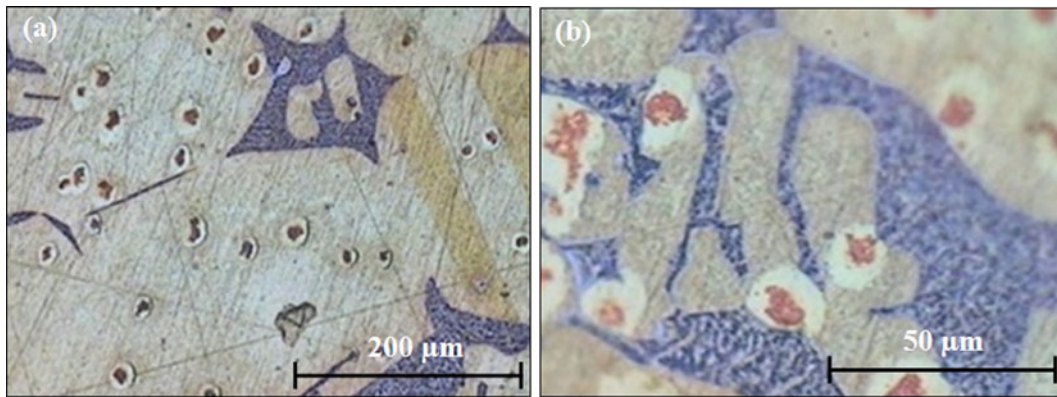


Figure 10. Corrosion attack on Cu-30Zn-1Sn in heat treatment condition A.

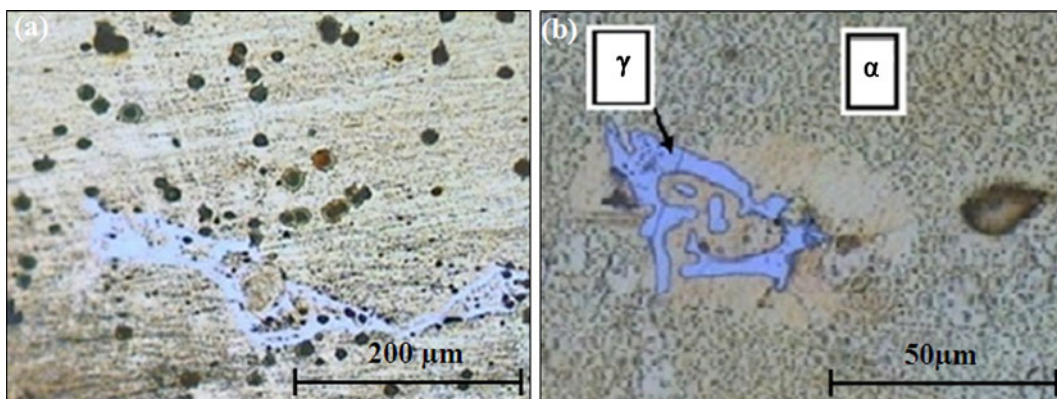


Figure 11. Corrosion attack on Cu-30Zn-1Sn in heat treatment condition C.

(Polunin *et al* 1982; Sohn and Kang 2002), where they proposed that Sn contributes in the passive surface layer. The present results revealed that in buffer solution containing chloride ions, SnO_2 oxide is only formed most likely on grain boundaries and improved their corrosion resistance.

In summary, in all conditions, local corrosion attack was not observed in Sn-rich phase. While in C, pits at α -phase surrounded by γ -phase are visible, in A, the β' -phase attack was not observed.

4. Conclusions

Effect of three different heat treatments viz. A, B and C, on the passivity of Cu-30Zn-1Sn brass was investigated. All heat treatments resulted mainly in formation of α , and Sn-rich phases as microstructure constituents. Beneficial effect of chloride ions on Cu-30Zn-1Sn alloy observed up to 0.05 M NaCl was attributed to the facilitated formation of copper oxide compounds and probable copper chloride complex. Passivity deterioration and pitting were observed at chloride concentrations higher than 0.05 M NaCl due to accelerated dissolution of copper and formation of copper chloride complexes such as CuCl_2^- . Adding tin improves the corrosion resistance by formation of Sn-rich (γ_1) phase in

grain boundaries. In buffer solution, the higher passivity current density observed in A was related to the small amount of β' . While in 1 M NaCl solution, the passivity current and breakdown potential of $4 \mu\text{A}/\text{cm}^2$ and -50 mV was monitored, respectively. Finally, preferential corrosion attack and consequently copper redeposition on α phase as matrix was observed.

Acknowledgement

Financial support and experimental facilities provided by Ferdowsi University of Mashhad are appreciated.

References

- Alfantazi A M, Ahmed T M and Tromans D 2009 *Mater. Des.* **30** 2425
- Asan A, Kabasakaloglu M, Isiklan M and Kılıc Z 2005 *Corros. Sci.* **47** 1534
- ASM handbook 2004a *Metallography and microstructure* (Ohio: ASM International) 9th ed., **Vol. 9**, pp 758, 759 and 1818
- ASM handbook 2004b *Heat treatment* (Ohio: ASM International) 9th ed., **Vol. 4**, pp 451, 1860 and 1960

- ASM handbook 2004c *Corrosion* (Ohio: ASM international) 9th ed., **Vol. 13**, p. 1508
- Crousier J and Bimaghra I 1989 *Electrochim. Acta* **34** 1205
- Effenberg H and Ilyenko S 2006 *Ternary alloy systems phase diagrams, crystallographic and thermodynamic data, materials science and international team evaluated by MSIT*, pp. 422–435
- Hansen M and Anderko K 1958 *Constitution of binary alloys* (New York: McGraw-Hill) 2nd ed., p. 650
- Heidersbach R H and Verink E D 1972 *Corrosion* **28** 397
- Jones D A 1992 *Principles and prevention of corrosion* (New York: Macmillan Publishing) p. 325
- Kabasakaloglu M, Kiyak T, Sendil O and Asan A 2002 *Appl. Surf. Sci.* **193** 167
- Mamas S, Kiyak T, Kabasakaloglu M and Koc A 2005 *Mater. Chem. Phys.* **93** 41
- Medusa thermodynamic software 2009 *Puigdomenech I* (<http://www.kemi.kth.se/medusa/>)
- Milosev I, Mikic T K and Gaberscek M 2006 *Electrochim. Acta* **52** 415
- Morales J, Fernandez G T, Esparza P, Gonzalez S, Salvarezza R C and Arvia A J 1995a *Corros. Sci.* **37** 211, 231
- Morales J, Fernandez G T, Esparza P, Gonzalez S, Salvarezza R C and Arvia A J 1995b *Corros. Sci.* **40** 177
- Newman R C, Shahrabi T and Sieradzki K 1988 *Corros. Sci.* **28** 873
- Polunin A V, Pchel'nikov A P, Losev V V and Marshakov I K 1982 *Electrochim. Acta* **27** 467
- Scendo M 2007 *Corros. Sci.* **49** 373
- Sherif E M and Park S M 2006 *Electrochim. Acta* **51** 4665
- Sherif E M, El-Shamy A M, Ramla M M and El-Nazhawy A O H 2007a *Mater. Chem. Phys.* **102** 231
- Sherif E M, Erasmus R M and Comins J D 2007b *J. Colloid. Interf. Sci.* **309** 470
- Sherif E M, Erasmus R M and Comins J D 2008 *Corros. Sci.* **50** 3439
- Sohn S and Kang T 2002 *J. Alloys Compd* **335** 281
- Toivanen R O, Hirvonen J and Lindroos V K 1985 *Nucl. Instrum. Meth.* **7–8** 200
- Zou J Y, Wang D H and Qiu W C 1997 *Electrochim. Acta* **42** 1733